



Mouro, J., Tiribilli, B., & Paoletti, P. (2018). A versatile mass-sensing platform with tunable nonlinear self-excited microcantilevers. *IEEE Transactions on Nanotechnology*.  
<https://doi.org/10.1109/TNANO.2018.2829404>

Publisher's PDF, also known as Version of record

License (if available):  
CC BY

Link to published version (if available):  
[10.1109/TNANO.2018.2829404](https://doi.org/10.1109/TNANO.2018.2829404)

[Link to publication record in Explore Bristol Research](#)  
PDF-document

This is the final published version of the article (version of record). It first appeared online via IEEE at <https://ieeexplore.ieee.org/document/8352046/> . Please refer to any applicable terms of use of the publisher.

## University of Bristol - Explore Bristol Research

### General rights

This document is made available in accordance with publisher policies. Please cite only the published version using the reference above. Full terms of use are available:  
<http://www.bristol.ac.uk/pure/about/ebr-terms>

# A versatile mass-sensing platform with tunable nonlinear self-excited microcantilevers

J. Mouro, B. Tiribilli, and P. Paoletti

**Abstract**—A versatile mass-sensing platform based on the nonlinear dynamical response of a microcantilever embedded in a self-excitation feedback loop is proposed. It is experimentally shown that the delay imposed in the feedback loop by an adjustable phase-shifter can be used to finely tune this system to work in three different modalities, according to the desired mass sensing application: i) as a continuous mass sensor, where the oscillation frequency smoothly responds to changes in the mass added to the resonator; ii) as a threshold sensor, where a sudden change in the oscillation frequency is triggered by an arbitrarily small change of mass added to the cantilever; and iii) as a stable microresonator, whose oscillation frequency is almost not affected by environmental conditions, such as changes in added mass, or in density/ viscosity of the surrounding fluid. This variety of dynamical responses was registered for a wide range of added masses, in the form of beads individually attached to the cantilever. A complete analytical model to explain the observed experimental results is derived and shows a strong agreement with the measured data. The high resolution and signal-to-noise ratio, as well as the threshold and stable sensing modalities obtained with this closed-loop technique, are not available in the current open-loop microcantilever-based mass sensors.

**Index Terms**—Mass-sensing, nonlinear oscillations, self-excited microcantilever.

## I. INTRODUCTION

Microelectromechanical systems (MEMS) have emerged in the last decades as the best candidates for a wide range of technological and scientific applications. Microresonator-based sensors, actuators or signal processing components benefit from the high resonance frequencies and quality

factors ( $Q$ ) characteristic of these mechanical resonators [1]. Their microscopic dimensions and very small active masses render these devices extremely sensitive to external perturbations from the surrounding environment, and were crucial to successfully develop imaging applications [2] or force [3], viscosity [4], temperature [5] and mass sensors [6], [7].

In particular, micromechanical resonators used for mass sensing have the potential to ultimately measure the mass of individual molecules, being only limited by the fundamental noise processes [6]. Typically, the operation of micromechanical mass sensors relies on detecting the resonance frequency shift induced by an additional mass adsorbed on the surface of the probe. The sensitivity is known to be greatly improved by using smaller devices, low-noise motion detection and ultrahigh vacuum. An extreme optimization of these parameters on a single experiment allowed achieving a yoctogram ( $10^{-24}$  g) resolution [7]. One of the major concerns that must always be addressed when developing a mass sensor is the reduced bandwidth – often less than 1 Hz [8] – due to the large quality factor of externally excited microresonators operating in air, which induces long transients. On the other hand, performing measurements in viscous fluids decreases the quality factors and the sensitivity, and often reveal the presence of the undesired spurious mechanical modes [9], [10]. When measuring the resonance frequency shift caused by the added mass of interest, it is usually assumed that the mass is distributed evenly on the probe surface, which is not necessarily true. In addition, when individual masses, such as cells or proteins, are attached, the response of the resonator depends on the actual position of the added mass [11]. Therefore, negative pressure in hollow cantilevers [12], mechanical traps [13] or centrifugal forces [14] were used to place the particles at a specific position along the probe.

More recently, strategies where the microresonator is embedded in a feedback loop proved to be very effective in obtaining a more selective frequency response, which can be crucial to overcome the low quality factor typically associated with viscous media and the undesired *forest of peaks*. Among the proposed strategies are the  $Q$ -control [15], parametric resonance [16], [17] and self-excitation circuits [18], [19]. In addition, using feedback loops makes the response of the resonator faster, which translates to a significant increase of measurement bandwidth. Generally, the resonance frequency of the device is continuously tracked by a frequency-modulated phase-locked loop (PLL), allowing measuring adsorption events in real time with sensitivities in the order of

This work was supported by EPSRC grant no. EP/N026799/1 on Self-Tuning Advanced Rheology Tool, and the CNR Short Term Mobility grants 2015 and 2016.

J. Mouro was with the department of Mechanical, Material and Aerospace Engineering, University of Liverpool, Brownlow Hill, Liverpool, L69 3GH, United Kingdom. He is now with the Department of Electrical and Electronic Engineering, University of Bristol, Woodland road, Bristol, United Kingdom.

P. Paoletti is with the department of Mechanical, Material and Aerospace Engineering, University of Liverpool, Brownlow Hill, Liverpool, L69 3GH, United Kingdom.

B. Tiribilli is with the Institute for Complex Systems, National Research Council (ISC-CNR), via Madonna del Piano 10, Sesto Fiorentino, Firenze I-50019, Italy.

Copyright © 2018 IEEE. Personal use of this material is permitted. However, permission to use this material for any other purposes must be obtained from the IEEE by sending a request to pubs-permissions@ieee.org.

atto- or zeptogram ( $10^{-18}$  to  $10^{-21}$  g) [20]-[22]. Applying the same concept for measuring multiple eigenmode frequencies simultaneously allows the determination of position and mass distribution of the analytes [23].

One of the main drawbacks of using feedback loops to improve sensing performance is the presence of different sources of nonlinearities introduced, for example, by the nonlinear electronic components required to process the signals or even by the intrinsic mechanical nonlinearities of the resonator. The analysis of the dynamics of microresonators in presence of mechanical nonlinearities has shown interesting and surprising phenomena, such as stable operation of the resonators far beyond the critical vibration amplitude [24], [25] or bistable regimes [26], [27]. It was also shown that the frequency of oscillation is strongly dependent on the delay affecting the feedback signal [27]-[29].

This work shows how shifting the signal along a self-excitation loop composed of a cantilever, a gain, a saturator and a tunable phase-shifter affects the dynamical response of the cantilever, and how it is possible to use this platform in three different regimes: as a high-sensitivity mass sensor, as a threshold mass sensor, and as a stable microresonator whose oscillation frequency is almost unaffected by the environmental conditions. The authors have previously studied and modeled a similar system in [29] and proposed it as a viscosity sensor in [30]. Here, such model is extended to incorporate the presence of the added mass, and the dynamical response of the cantilever is theoretically and experimentally studied as function of the added mass (in the form of attached beads) and of the feedback delay that is introduced in the loop by the phase-shifter.

The paper is organized as follows: in section II the experimental setup is discussed. Special emphasis is given to the description and characterization of the phase-shifter, and to the methods of attaching and measuring the diameters and mass of the beads used to change the mass of the resonator. Experimental results illustrating the nonlinear behavior of the self-excited oscillation frequency for different added masses and delays in the feedback loop are presented in section III. In section IV the nonlinear response of the cantilever is discussed by analyzing the phase condition for the existence of self-sustained oscillations and an analytical model describing the dependence between the self-sustained oscillation frequencies and the added mass is derived. Finally, some conclusions are discussed in section V.

## II. EXPERIMENTAL METHODS

### A. Experimental setup

A schematic of the experimental setup used to study the dynamics of the sensor operating in air is shown in Fig. 1(a). Glass and polystyrene beads are individually attached to the cantilever to change the effective mass of the probe. The cantilever motion is acoustically excited by a dither piezo and optically detected by a four-quadrant detector connected to a R9 controller (RHK Technology). The switch S indicates the possibility of selecting between two different measuring

configurations: traditional amplitude modulation or open-loop mode (AM in Fig. 1), and autotapping or closed-loop mode (AT in Fig. 1). In the open-loop mode, the dither piezo is externally excited by a function generator, using sinusoidal signals at different frequencies. The amplitude and phase of the deflection signal are measured using a lock-in. Both the function generator and the lock-in are available in the R9 controller itself. In the closed-loop mode, the deflection signal coming from the detector is fed into an electronic circuit (Elbatech srl) composed of a tunable phase-shifter, a gain and a saturator, before being fed back to the excitation dither piezo as a voltage to induce the self-oscillations of the cantilever. The amplitude and frequency of these oscillations are measured from reading the deflection signal with an external oscilloscope (Tektronix TDS-2022).

The total delay,  $\tau_{tot}$ , shown in Fig. 1(a) represents the intrinsic delay of the feedback loop, i.e. the time that the deflection signal naturally takes to go around the feedback loop once. This delay is responsible of shifting the initial sinusoidal deflection signal by several periods. It was shown in [29] that the total delay,  $\tau_{tot}$ , results from individual contributions of the electronic components of the circuit (gain + saturator),  $\tau_{ET}$ , the electronic elements composing the phase-shifter,  $\tau_{PS}$ , and the delay caused by the propagation of the elastic waves in the cantilever and holder materials,  $\tau_{CT}$ . The first two terms,  $\tau_{ET}$  and  $\tau_{PS}$ , were individually estimated in [29] by connecting sinusoidal signals to the inputs of these circuits and measuring the phase shift of the corresponding outputs. The last term of the total delay,  $\tau_{CT}$ , depends on the specific connection between the cantilever and the holder, and must be measured every time a new probe is used.

The adjustable phase-shifter introduced in the feedback loop allows adding an extra phase shift to the natural phase shift induced by the total delay of the system. Its role is to finely control the phase between the cantilever deflection and the dither piezo excitation. Fig. 1(b) shows the electrical schematics of a single stage of the phase-shifter, which works as an all-pass filter capable of shifting the signal by at most  $-\pi$  radians. The complete phase-shifter consists of two of these stages connected in series (inducing a total phase shift of  $-2\pi$  radians), each stage being individually operated by adjusting a potentiometer which controls the value of a resistor,  $R_i$ , between 0 and 10.2 k $\Omega$ . The values of the capacitances of each stage,  $C_i$ , are fixed in the circuit and are chosen accordingly to the working range of frequencies, to guarantee that at least one of the stages can effectively reach the maximum phase shift of  $-\pi$  radians. Finally, there is also the possibility of inverting the polarity of the voltage signal applied to the terminals of the dither piezo, as shown by the parameter  $p = \pm 1$  of Fig. 1(a). This option allows users to shift the signal by extra  $-\pi$  radians. To summarize, the two stages of the phase-shifter, combined with the possibility of inverting the polarity of the signal that feeds the piezo, can be used to adjust the phase-shift of the signal along the feedback loop by a complete period ( $-2\pi$  radians). Note that this shift will add to the shift caused by the intrinsic total delay of the system,  $\tau_{tot}$ . The influence of

feedback delay on the dynamic response of the cantilever with different added masses will be assessed in this work.

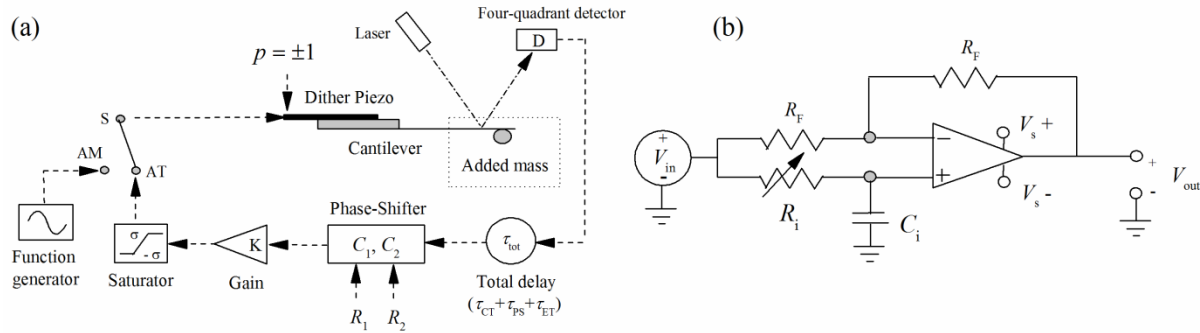


Fig. 1. a) Schematic of the experimental setup. A glass/polystyrene bead is attached to the silicon cantilever. The cantilever motion is acoustically excited by a dither piezo and optically detected using a four-quadrant detector. In amplitude mode (AM), or open-loop mode, the function generator sweeps the excitation driving frequency, and deflection amplitude and phase are recorded. In autotapping mode (AT), or closed-loop mode, the deflection signal is fed back to the piezo as a voltage, after being shifted by the total delay and by an adjustable phase-shifter, amplified by the gain and limited by the saturator in the feedback loop. The polarity of the voltage applied to the dither piezo can be inverted ( $p = \pm 1$ ). b) Detail of a single stage of the phase-shifter, capable of shifting the signal by at most  $-\pi$  radians. Two stages were connected in series. The values of  $C_1$  and  $C_2$  are 237 pF and 5.14 nF in each stage, respectively, and the two potentiometers  $R_1$  and  $R_2$  are adjustable within the range 0-10.2 k $\Omega$ .

The closed-loop configuration shown in Fig. 1(a) generates self-sustained stable oscillations of the cantilever with angular frequency  $\omega_{osc}$ . The onset of the self-oscillations results from a competition between the feedback gain, which constantly amplifies the motion of the cantilever, and the presence of the nonlinear saturation, which constantly limits these trajectories. When the system reaches a steady-state, the cantilever self-oscillates with a frequency and amplitude ensuring that the overall loop gain is unitary and that the total phase shift of the signal around the feedback loop is an integer multiple of  $-2\pi$  radians, see section IV [29], [30].

In this work, the dynamic response of the silicon ACST cantilever (from AppNano) vibrating in air with five different beads attached was characterized using the open-loop and closed-loop configurations. The cantilever natural resonance frequency (in air and with no mass attached) was measured using the open-loop configuration. The length and width of the cantilever were measured from visual inspection on the microscope using the calibrated micrometer ruler shown in Fig. 2(a). Finally, the thickness, fundamental resonance frequency and spring constant were estimated as described in section II. Table I shows the estimated and measured geometrical and dynamical parameters of the cantilever.

TABLE I  
GEOMETRICAL AND DYNAMICAL PARAMETERS OF ACST  
CANTILEVER MEASURED EXPERIMENTALLY

ACST (AppNano)	
Length ( $\mu\text{m}$ )	160
Width ( $\mu\text{m}$ )	33
Thickness ( $\mu\text{m}$ ) (eq. (1))	2.91
Frequency (kHz)	162.32
Spring Constant (N/m) (eq. (4))	8.92

### B. Attaching the beads

Different micrometric beads of glass (Monospheres, Whitehouse Scientific LTD) or polystyrene (Latex beads polystyrene, Sigma-Aldrich) were individually attached to the free-end of the cantilever. The attached beads work as a concentrated mass of a known material, located at a known position along the cantilever. This approach is crucial to perform repeatable experiments and to validate the analytical model. More complex strategies to add mass to the cantilever, such as deposition techniques or chemical reactions on the surface, would make it difficult to control, for example, the thickness or stress of the added layer which can change the stiffness and resonance frequency of the cantilever.

For such validation purpose, a simple process to attach the individual beads was developed: a very small amount of beads were randomly spread on a clean microscope slide and put underneath the cantilever. This tipless cantilever is part of an AFM setup and its in-plane position and height can be regulated using two micrometric screws. An optical microscope was then placed on top of this apparatus and focused on the beads distributed on the microscope slide. To attach the beads, the cantilever was carefully moved down and laterally, while looking through the microscope, until the center of its free-end on the bottom surface went in contact with one single isolated bead. Finally, at this point, an extra slight movement down of the cantilever is used to apply a small pressure to the bead and facilitate the attachment. This contact was perceptible on the microscope by the bending of the cantilever. The cantilever was then brought up using the micrometric screws and most of the times the chosen bead was found attached to the probe bottom surface (the large ratio between cantilever surface and volume of the beads contribute favorably to the attachment, due to surface electrostatic forces) [31]. To confirm the attachment, the microscope slide underneath the cantilever was substituted by a mirrored surface, which allows to observe the bottom

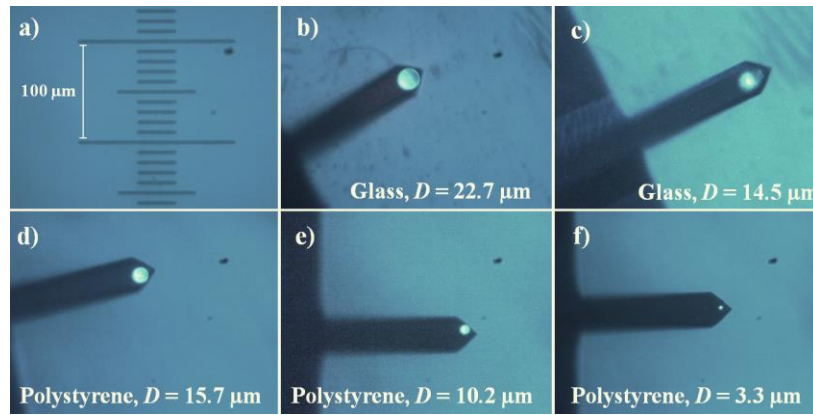


Fig. 2. Optical images of the beads attached to bottom surface of the cantilever and the respective diameters estimated optically. a) Calibration slide used to estimate the dimensions of the cantilever (length and width) and diameter of beads; b) and c) big and small glass beads, respectively; d, e, f) Big, medium and small beads of polystyrene, respectively. All the images have the same magnification.

side of the cantilever with the attached bead. Some images of the different beads, shown in Fig. 2, were recorded with a camera connected to the microscope. To cover several orders of magnitude of added masses, five beads of different sizes and two different materials were individually attached to the tip of the cantilever: one *small* and one *big* bead of glass, and one *small*, one *medium* and one *big* bead of polystyrene.

### C. Measuring mass and diameter of the beads

#### 1) Optical estimation of bead diameter and mass

The diameters of the beads were estimated from the images acquired on the microscope using a CCD camera (Basler acA250014gc) at 2590x1942 pixels. The reported bead diameter is the mean value of the width of three different profiles, processed using the free software *Gwyddion* [32] and compared with the image of a calibrated micrometric ruler (AmScope MR095 Microscope Stage Calibration Slide). The micrometric ruler and the five beads attached with the respective estimated diameters are shown in Fig. 2.

The optical estimation of the beads diameter (with associated error) is shown in Table II. The mass of the beads was then calculated from the optically estimated diameter of each bead, considering the density of the materials [33], [34] and assuming that the beads are perfect spheres.

#### 2) From the resonance frequency of the cantilever with the beads attached

An alternative way of determining the mass and diameter of each bead is based on the resonance frequency of the cantilever with the beads attached (measured in open-loop mode). This method allows a more complete characterization of the cantilever, which is useful for the modeling performed in later sections. The cantilever thickness can be determined from the Euler-Bernoulli beam equation with the appropriate boundary conditions [35], using the value of resonance frequency of the cantilever in air and with no added mass measured in open-loop mode ( $f_0 = \frac{\omega_0}{2\pi} = 162.32 \text{ kHz}$ ) and the optically estimated length  $L$  of the beam:

$$T = \omega_0 \frac{L^2}{(1.8751)^2} \sqrt{\frac{12\rho_{CT}}{E}} = 2.91 \mu\text{m}. \quad (1)$$

In this equation,  $E = 179 \text{ GPa}$  and  $\rho_{CT} = 2330 \text{ kg/m}^3$  are the Young's modulus and the density of the silicon, respectively. The calculated value of thickness is reported in Table I.

In this work, the cantilever is modeled as a single-degree-of-freedom damped harmonic oscillator, with an added mass and subject to a hydrodynamic force. This model is an extension of the model presented in reference [30], in which the cantilevers oscillated in viscous fluids. The total hydrodynamic force is described by an inertial and a dissipative term, which account, respectively, for the weight of the layer of fluid that the beam displaces as it moves, and for the viscous drag force exerted by the fluid on the moving cantilever [36]. These two terms can therefore be modeled as a hydrodynamic mass,  $m_{hydro}$ , and a hydrodynamic damping coefficient,  $c_{hydro}$ , and approximated by [30], [36]-[38]:

$$m_{hydro}(\omega) = \frac{\pi}{4} \rho W^2 L \left( a_1 + \frac{a_2}{W} \sqrt{\frac{2\eta}{\rho\omega}} \right) \quad (2)$$

$$c_{hydro}(\omega) = \frac{\pi}{4} \rho W^2 L \omega \left( \frac{b_1}{W} \sqrt{\frac{2\eta}{\rho\omega}} + \frac{2\eta}{\rho\omega} \left( \frac{b_2}{W} \right)^2 \right). \quad (3)$$

Both hydrodynamic parameters depend on the angular frequency of oscillation  $\omega$ , the viscosity  $\eta$  and density  $\rho$  of the surrounding fluid, and on the constants  $a_1 = 1.0553$ ,  $a_2 = 3.7997$  and  $b_1 = 3.8018$  and  $b_2 = 2.7364$ . Finally,  $L$  and  $W$  represent, respectively, the length and width of the cantilever measured optically and shown in Table I.

According to the harmonic oscillator model, the resonance frequency of the cantilever vibrating in air and with no added mass is given by  $\omega_0 = \sqrt{k/m_{r,0}}$ , where  $k$  is the spring constant of the cantilever and  $m_{r,0}$  accounts for the effective mass concentrated on the tip of the cantilever with no bead attached (the index 0 is used hereafter to denote the case where no bead is attached).

This expression is used to calculate the spring constant of the cantilever, knowing that  $f_0 = 162.32 \text{ kHz}$  and considering that  $m_{r,0} = 0.24 (m_{CT} + m_{hydro}(\omega_0))$  [39]:

$$k = \omega_0^2 0.24 (m_{CT} + m_{hydro}(\omega_0)) = 8.92 \text{ N/m}, \quad (4)$$



where  $m_{CT} = TLW\rho_{CT} = 3.53 \cdot 10^{-11} \text{ kg}$  is the total mass of the cantilever and  $m_{hydro}(\omega_0)$  is substituted by the expression given by (2), considering the frequency  $\omega_0$  and the properties of the air ( $\eta \approx 1.8 \times 10^{-5} \text{ Pa s}$  and  $\rho \approx 1.29 \text{ kg/m}^3$  [40]). The calculated value of  $k$  is presented in Table I. It is worth noting that the value of the spring constant obtained with this method ( $k = 8.92 \text{ N/m}$ ) is in close agreement with the value obtained by the well-known expression  $k = \frac{EWT^3}{4L^3} = 8.95 \text{ N/m}$  [35].

Finally, the resonance frequency of the cantilever vibrating with the different beads,  $f_A$ , (measured in each case using the open-loop mode) is used to determine the added mass of the beads,  $m_A$ , using the expression  $\omega_A = \sqrt{k/m_{r,A}}$ , where  $m_{r,A} = 0.24 \left( m_{CT} + m_{hydro}(\omega_A) \right) + m_A$  is the effective mass concentrated on the tip of the cantilever [41] and  $k$  is the spring constant of the cantilever, calculated from (4) (the index  $A$  is hereafter used to denote the presence of an added mass). By rearranging the previous expression, one obtains:

$$m_A = \frac{k}{\omega_A^2} - 0.24 \left( m_{CT} + m_{hydro}(\omega_A) \right). \quad (5)$$

Theoretically, this expression is only valid when the beads are perfectly placed at the free end of the cantilever, which is not always the case here, as shown in Fig. 2. The position of the bead along the major axis of the cantilever changes its resonance frequency and, therefore, the added mass calculated with (5). References [12] and [41] discuss a method to correct for this effect, based in shape of the vibrating mode. In the experiments described here, the error between values of mass added to the cantilever obtained using both methods was found to be within the experimental error of the setup and therefore this correction was discarded for the sake of simplicity. The diameter of each bead can then be calculated from its mass, assuming that the bead is a perfect sphere and considering the density of each material [32], [33]. The values of masses and diameters obtained with this method are shown in Table II and show a good agreement with the values obtained from visual inspection.

### III. EXPERIMENTAL RESULTS

#### A. Open-loop Mode – Amplitude and Phase Spectra

Fig. 3 shows a representative example of the experimental amplitude and phase spectra obtained by sweeping the excitation frequency in the open-loop configuration, for the case of the ACST cantilever with the medium polystyrene bead attached. The measured amplitude spectrum is fitted to the amplitude of the damped harmonic oscillator model, given by the function [8], [42]:

$$A = \frac{H}{\sqrt{(\omega_A^2 - \omega^2)^2 + \left(\frac{\omega\omega_A}{Q_A}\right)^2}}, \quad (6)$$

where  $A$  is the measured amplitude,  $\omega$  is the excitation angular frequency of the dither piezo,  $\omega_A$  is the angular resonance frequency of the cantilever with the added bead (the index  $A$

should be substituted by the index  $0$  in the case of no added mass),  $Q$  and  $H$  are the quality factors and amplitude of the resonant mode, respectively. The parameters  $\omega_A$ ,  $Q_A$  and  $H$  were used to fit the model of (6) to the experimental amplitude spectra, as exemplified in Fig. 3(a). The fitted values of resonance frequency,  $f_A$ , are used to calculate the mass of each bead using (5) and are shown in Table II, along with the values of  $Q_A$ . Fig. 3(b) shows the phase spectra measured in open-loop mode and used to estimate the delay due to the cantilever and its holder,  $\tau_{CT}$ . This delay is the proportionality constant between the excitation angular frequency  $\omega$  and the phase shift between the input excitation signal fed to the piezo and the output deflection signal. In open-loop mode the feedback loop is open and the measured delay just contains information about the mechanical cantilever and holder, excluding the influence of all other electronic components.  $\tau_{CT}$  is then estimated from the slope of the phase spectrum far from the resonance (to avoid the characteristic jump of  $-\pi$  radians of this region) using:

$$\varphi_{delay} = -\tau_{CT}\omega, \quad (7)$$

with  $\varphi_{delay}$  in radians, refer to Fig. 3(b). An average delay of  $\tau_{CT} \approx 13.9 \mu\text{s}$  was obtained considering the measurements in open-loop mode of the cantilever with the different beads.

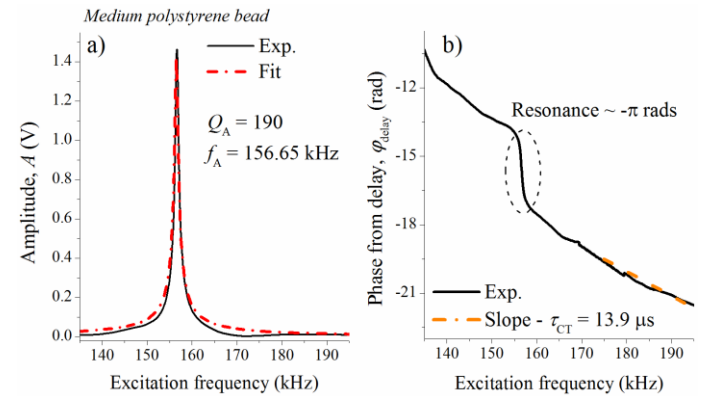


Fig. 3. Experimental amplitude and phase measured in open-loop mode for the cantilever with the medium polystyrene bead attached. a) The damped harmonic oscillator model is fitted (red dashed-dotted line) to the measured amplitude (solid black line) and the parameters are extracted; b) The delay on the propagation of the elastic waves through the holder and cantilever materials is extracted from the slope of the phase spectrum away from the resonance. The resonance occurs at 156.65 kHz, as indicated in Table II.

#### B. Closed-loop Mode – Oscillation frequencies as function of signal shift along the loop, for different added masses

Following the characterization in open-loop mode, the dynamics of cantilever with (or without) the beads operating in the closed-loop configuration was studied as a function of the phase shift imposed by the adjustable phase-shifter,  $\varphi_{PS}$ . This shift can be controlled by adjusting the two potentiometers  $R_1$  and  $R_2$  in the phase-shifter shown in Fig. 1 and by inverting the polarity of the signal fed to the dither piezo.

TABLE II  
DIAMETERS AND MASSES OF BEADS ATTACHED OBTAINED WITH THE TWO PROPOSED METHODS.

	Beads	$D_{bead} \pm 0.5 (\mu m)$ (optically)	$m_A (kg)$ (sphere)	$f_A (kHz)$ (Eq. (6))	$Q_A$ (Eq. (6))	$m_A (kg)$ (Eq. (5))	$D_{bead} (\mu m)$ (sphere)	% error on $D (\mu m)$
No bead	-	-	-	162.32	200	-	-	
Polystyrene ( $\rho = 1050 \text{ kg/m}^3$ )	Small	3.3	$1.98 \times 10^{-14}$	161.15	200	$1.83 \times 10^{-14}$	3.2	3%
	Medium	10.2	$5.83 \times 10^{-13}$	156.65	190	$5.25 \times 10^{-13}$	9.9	3%
	Big	15.7	$2.13 \times 10^{-12}$	145.65	180	$1.97 \times 10^{-12}$	15.3	2.5%
Glass ( $\rho = 2450 \text{ kg/m}^3$ )	Small	14.5	$3.91 \times 10^{-12}$	131.35	130	$4.41 \times 10^{-12}$	15.1	4%
	Big	22.7	$1.50 \times 10^{-11}$	98.27	50	$1.47 \times 10^{-11}$	22.5	1%

A typical experimental protocol consisted in fixing the value of polarity ( $p = 1$ ) and the value of  $R_1$ , and sweeping the value of  $R_2$  from 0 to 10.2 k $\Omega$ .

Then the value of  $R_2$  was kept constant while the value of  $R_1$  was swept until reaching 10.2 k $\Omega$ . At this stage, the polarity of the piezo was inverted ( $p = -1$ ) and the potentiometers were sequentially swept back to 0 k $\Omega$ . For each set of experimental conditions the frequency and amplitude of the oscillation were recorded.

By sweeping the values of the resistors and inverting the polarity on the piezo, the original signal (deflection signal from the four-quadrant detector) can be shifted by at least a complete period ( $-2\pi$  radians), before being fed back to the dither piezo.

Fig. 4 presents examples of experimental results obtained with the cantilever with the medium polystyrene bead attached.

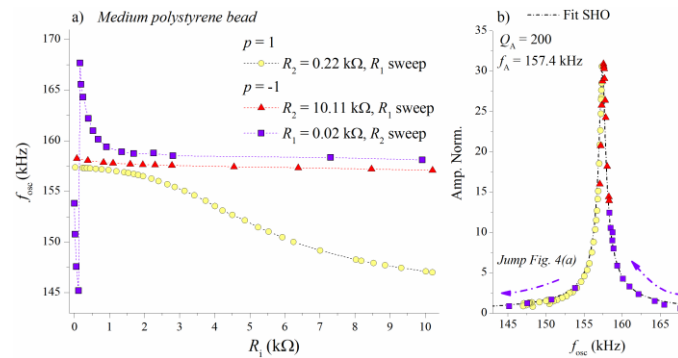


Fig. 4. Frequencies and amplitudes of the self-sustained oscillations, using the medium polystyrene bead attached to the cantilever. a) Frequencies of self-excited oscillation as a function of the value of one resistor in the phase-shifter, for fixed polarities. The dotted lines are guidelines to the eye; b) Amplitude of self-oscillations against the corresponding oscillation frequency for each set of experimental conditions. The dashed arrows indicate the rapid frequency decrease around the sudden jump (from 145.0 kHz to 167.5 kHz), also shown in Fig. 4(a) (purple squares).

Fig. 4(a) shows three series of results obtained when sweeping  $R_1$  or  $R_2$ , for fixed polarities. Three distinct behaviors, depending on the experimental conditions, can be observed: the series represented by the yellow circles shows a steady decrease on the values of the oscillation frequencies when  $R_1$  increases, for non-inverted polarity. Inverting the polarity, the red triangles show little dependence of the oscillation frequencies with the value of the resistor  $R_1$ . Finally, the purple squares show a steep decrease on the values of oscillation frequencies for low values of increasing  $R_2$ , before an abrupt jump from low to high frequencies is observed. Then, the steep decrease of oscillation frequencies resume,

until a plateau is reached. On the right panel, the amplitude is plotted against the corresponding oscillation frequency, for each set of experimental conditions. It can be observed that this amplitude curve recovers the shape of the amplitude curve measured in the open-loop configuration (Fig. 3(a)) and it can also be fitted by the harmonic oscillator model with similar parameters.

The best way to compare all the measured experimental data is by showing the shift imposed by the phase-shifter in the loop for each set of fixed experimental conditions ( $R_1$ ,  $R_2$  and  $p$ ), against the corresponding oscillation frequency. This is shown in Fig. 5, for each attached bead. The shift imposed by the phase-shifter is calculated using (8), explained in detail in section IV, which contains all the experimental parameters ( $R_1$ ,  $R_2$  and  $p$ ). The black dashed line represents the case of the cantilever with no added mass and the symbols represent the cases with the different beads attached. It can be observed that, as the added mass increases, the position of the jump moves to more negative values of imposed shift by the phase-shifter. The case of the green squares, representing the big glass bead, is the exception. The reason, as explained in the next section, is the periodicity of  $-360$  degrees on the response of the self-excited cantilever – in other words, the signal circulating in the feedback loop can only be shifted by a maximum of  $-2\pi$  radians, before repeating itself.

It can also be noted that the values of oscillation frequency away from the abrupt jump tend to the values of the natural resonance frequency of the cantilever with each bead attached (see Table II). The data shown in Fig. 4(a) is contained in the purple squares of Fig. 5 (medium polystyrene bead). In particular, for the case of the experimental data that shows the sudden jump in Fig. 4(a) ( $p = -1$ ,  $R_1 = 0.02$  k $\Omega$  and  $R_2$  sweep), one can conclude that by increasing the value of the potentiometer  $R_2$  while keeping the other parameters constant, the frequency of the self-sustained oscillations decrease from 154 kHz to 145 kHz (moving away from the cantilever resonance frequency, see Fig. 4), corresponding to an increased phase-shift imposed by the phase-shifter in the loop (Fig. 5). At about  $-250$  degrees of phase-shift (Fig. 5, or  $R_2 \sim 0.01$  k $\Omega$  in Fig. 4(a)), the oscillation frequency jumps abruptly to a higher value of 167.5 kHz (Fig. 4 and Fig. 5). This jump corresponds to the oscillations in the loop *emerging* on the right side of the resonance peak of the cantilever, with low amplitude (Fig. 4(b)). Finally, further increasing the phase-shift causes the frequency and amplitude of the oscillations to increase, while approaching the natural frequency of the cantilever (Fig. 4(b)).

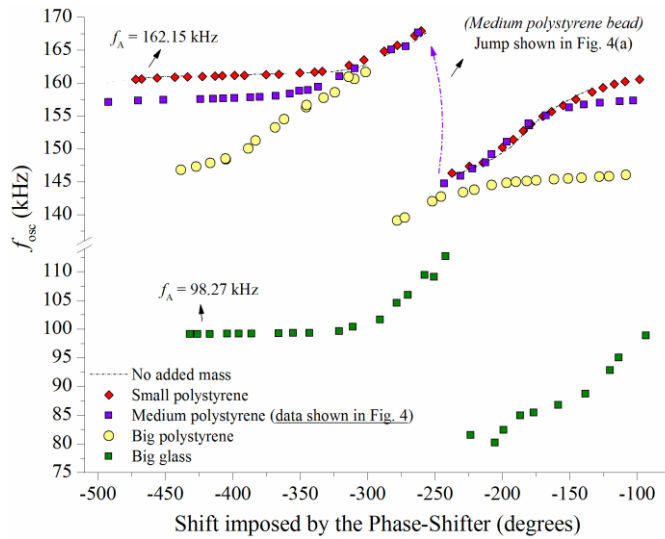


Fig. 5. Cantilever oscillation frequencies plotted against the shift imposed by the phase-shifter (calculated with (8)), for each set of experimental conditions ( $R_1$ ,  $R_2$  and  $p$ ). The position of the jump moves to more negative values of imposed shift as the added mass increases. The values of oscillation frequency far from the jump tend to the values of the natural resonance frequency of the cantilever with the added masses. (To improve the clarity of the figure the case of the small glass bead is not shown).

In conclusion, the experimental data shown in Fig. 4 shows that there are sets of experimental conditions that can make the response of this system very stable, i.e. insensitive to changes in imposed shifting delay by the phase-shifter. There are also different operating conditions that can make the oscillation frequencies to respond very fast to changes in imposed delay, or even to jump abruptly for small variations of the imposed delay. The concept behind using this system as a versatile mass-sensing platform is the possibility to *choose* the operating conditions to make the system work in one of these three distinct ways, and use the masses added to the cantilever to change the phase of the system (playing the role of the phase-shifter). In the next section these results will be modeled and explained.

#### IV. ANALYTICAL MODELING AND INTERPRETATION OF THE EXPERIMENTAL RESULTS

An analytical model of the self-excitation loop is developed in this section and used to interpret the experimental results shown in section III. The model studies the effect of each individual circuit element on the phase of the signal circulating in the excitation loop and the conditions that must be verified to obtain self-sustained oscillations.

##### A. Phase of the cantilever vibrating in viscous fluid with an arbitrary added mass

The phase of the cantilever vibrating in a viscous fluid with an arbitrary added mass,  $m_A$ , is calculated using the transfer function of the damped harmonic oscillator shown in (6) [30], [41]:

$$\varphi_{CT} = -\text{atan}\left(\frac{\omega\gamma}{\omega_A^2 - \omega^2}\right) = -\text{atan}\left(\frac{\omega(c+c_{hydro})}{k - \omega^2(0.24(m_{CT}+m_{hydro})+m_A)}\right), \quad (7)$$

where  $\varphi_{CT}$  is the phase of the cantilever (i.e. between force applied to its base and resulting deflection at the free end),  $\gamma = (c + c_{hydro}) / (0.24(m_{CT} + m_{hydro}) + m_A)$  is the damping ratio of the cantilever with the added mass  $m_A$ ,  $\omega$  is the angular frequency of oscillation and  $\omega_A$  is the angular resonance frequency of the cantilever with the added mass (the index  $A$  should be substituted by the index  $0$  and  $m_A = 0$  in the case of no added mass), and with  $m_{hydro}$  and  $c_{hydro}$  given by (2) and (3). Finally,  $k$  is the spring constant of the cantilever, determined from (4), and  $c = \frac{\omega_0 m_{CT}}{Q_0}$  is the intrinsic viscous damping coefficient, obtained from the fit of the damped harmonic oscillator model to the experimental amplitude of the cantilever with no attached mass in open-loop configuration [30], [41]. When the cantilever vibrates in a viscous medium this parameter is often negligible compared to  $c_{hydro}$ . The dashed-dotted orange curve of Fig. 6 represents the cantilever phase calculated numerically using (7), as function of the oscillation frequency, for the case of no added mass to the cantilever. The geometry of the cantilever shown in Table I and the rheological properties of air [40] were considered in the simulation. The presence of the cantilever in the feedback loop will cause a shift in the interval  $0$  and  $-\pi$  radians between the excitation force and the mechanical deflection.

##### B. Phase of the elements of the electronic circuit

The elements of the electronic circuit are the gain, the saturator, the total intrinsic delay of the loop and the adjustable phase-shifter. The saturator is the only nonlinear block of the feedback loop. Nevertheless, the output of the nonlinear saturator can be well approximated by a sinusoidal wave having the same frequency as the input, due to the intrinsic band-pass filter characteristics of the resonator embedded in the feedback loop. In other words, the presence of the resonator in the feedback loop attenuates any low frequencies or higher harmonics of the signal caused by nonlinear elements. Therefore, the saturator can be substituted with an amplitude-dependent gain by using the describing function technique [29], [43]. In this case, if the amplitude of the input signal is smaller than the threshold  $\sigma$  (representing the saturation threshold value defined by the user and shown in Fig. 1(a)), the gain is unitary and the output signal is the same as the input. When the amplitude of the input is higher than  $\sigma$ , the output becomes smaller than the input, which contributes to stabilizing the signal that is constantly amplified by the feedback gain. The gain  $K$  and the saturator describing function are real functions for each value of amplitude and frequency of the self-sustained oscillation [29], [43]. Therefore, these elements act only on the amplitude of the signal and do not affect its phase.

Conversely, the intrinsic total delay of the setup introduces a natural shift of the signal given by  $\varphi_{tot} = \tau_{tot}\omega_{osc}$ , with  $\varphi_{tot}$  in radians, where  $\omega_{osc}$  is the angular oscillation frequency. The delay  $\tau_{tot}$  is the sum of three distinct contributions, see section II. The first two terms were measured in [29], where



this electronic circuit was used for the first time ( $\tau_{PS} = 1.0 \mu s$  and  $\tau_{ET} = 1.1 \mu s$ ). The delay introduced by the cantilever and holder,  $\tau_{CT}$ , was measured in section III from the phase curve in the open-loop configuration ( $\tau_{CT} = 13.9 \mu s$ ). Therefore,  $\tau_{tot} = \tau_{PS} + \tau_{ET} + \tau_{CT} = 16.0 \mu s$ . The dotted green line in Fig. 6 represents the total delay of the system plotted against the oscillation frequency.

Finally, the phase-shifter can be described by the transfer function  $PS(j\omega) = pH_1(j\omega_{osc})H_2(j\omega_{osc})$ , where  $H_i(j\omega_{osc}) = \frac{1-j\omega_{osc}R_iC_i}{1+j\omega_{osc}R_iC_i}$  is the transfer function of each stage. Therefore, the total shift imposed by the phase-shifter reads:

$$\varphi_{PS} = \pi P - 2 \operatorname{atan}(\omega_{osc}R_1C_1) - 2 \operatorname{atan}(\omega_{osc}R_2C_2), \quad (8)$$

with  $\varphi_{PS}$  in radians, and the parameter  $P$  used to model the inversion of polarity in the dither piezo (for convention,  $p = 1$  and  $P = 0$  for non-inverted polarity and  $p = -1$  and  $P = -1$  for inverted polarity). In this work,  $C_1 = 237 pF$  and  $C_2 = 5.14 nF$ . Examples of the shift created by one stage of the phase-shifter with inverted polarity are shown in blue in Fig. 6.

The total shift of the signal imposed by the electronic circuit,  $\varphi_{elec}$ , for fixed experimental conditions, results from contributions of all the described elements and reads:

$$\varphi_{elec} = \pi P - 2 \operatorname{atan}(\omega_{osc}R_1C_1) - 2 \operatorname{atan}(\omega_{osc}R_2C_2) - \omega_{osc}\tau_{tot}. \quad (9)$$

### C. Phase condition for the existence of self-sustained oscillations in the feedback loop

The existence of self-sustained oscillations in the feedback loop implies that the deflection signal repeats itself after a complete loop in the self-excitation scheme. Formally, this condition can be stated as [28], [29]:

$$\begin{aligned} y(t) &= K\psi(a)pCT(j\omega)PS(j\omega)e^{-j\omega\tau_{tot}}y(t) \\ \Rightarrow K\psi(a)pCT(j\omega)PS(j\omega)e^{-j\omega\tau_{tot}} &= 1, \end{aligned} \quad (10)$$

where  $y(t)$  represent the probe deflection,  $CT(j\omega)$ ,  $PS(j\omega)$  and  $e^{-j\omega\tau_{tot}}$  are the transfer functions of the cantilever, phase-shifter and total delay of the setup, respectively, the parameter  $p = \pm 1$  accounts for the polarity applied on the terminals of the dither piezo,  $K$  represent the gain and  $\psi(a)$  is the describing function of the saturator used in the experimental feedback loop, with  $a$  being the amplitude of the saturator input [29], [43]. Given that the gain  $K$  and the describing function of the saturator  $\psi(a)$  [42] are real functions and do not affect the phase of the signal, (10) can be decomposed into its real and imaginary parts as:

$$K\psi(a)\operatorname{Re}[G(j\omega)] = 1, \quad (11)$$

$$\operatorname{Im}[G(j\omega)] = 0, \quad (12)$$

where  $G(j\omega) = pCT(j\omega)PS(j\omega)e^{-j\omega\tau_{tot}}$ . Equation (11) shows that the overall loop gain must be unitary, while (12) states that the total phase shift around the loop must be an

integer multiple of  $2\pi$  radians. By decomposing the total phase of the transfer function  $G(j\omega)$  and using (9), equation (12) can be rewritten as:

$$\varphi_{CT} + \varphi_{elec} = 0 \pmod{2\pi}. \quad (13)$$

where  $\varphi_{CT}$  is the phase of the cantilever oscillating at  $\omega_{osc}$ . Equation (13) describes the phase condition for the existence of self-sustained oscillations. It shows that the cantilever will adjust its phase (and hence its oscillation frequency  $\omega_{osc}$ ) in order to compensate the total phase,  $\varphi_{elec}$ , imposed by the phase-shifter (function of  $R_1$ ,  $R_2$  and  $\omega_{osc}$ ), the polarity on the piezo (function of  $P$ ) and the total intrinsic delay of the system (function of  $\omega_{osc}$  and  $\tau_{tot}$ ).

Fig. 6 illustrates how (13) can be used to explain the observed experimental results shown in section III. This figure shows the phase associated with each element of the circuit plotted against the oscillation frequency, as described in section IV.B. The overall phase is then calculated by adding all the terms together. The values of frequency for which the overall phase matches a multiple of  $-2\pi$  radians are the solutions of (13). These solutions are represented by the black circles on top of the dashed-dotted red horizontal lines.

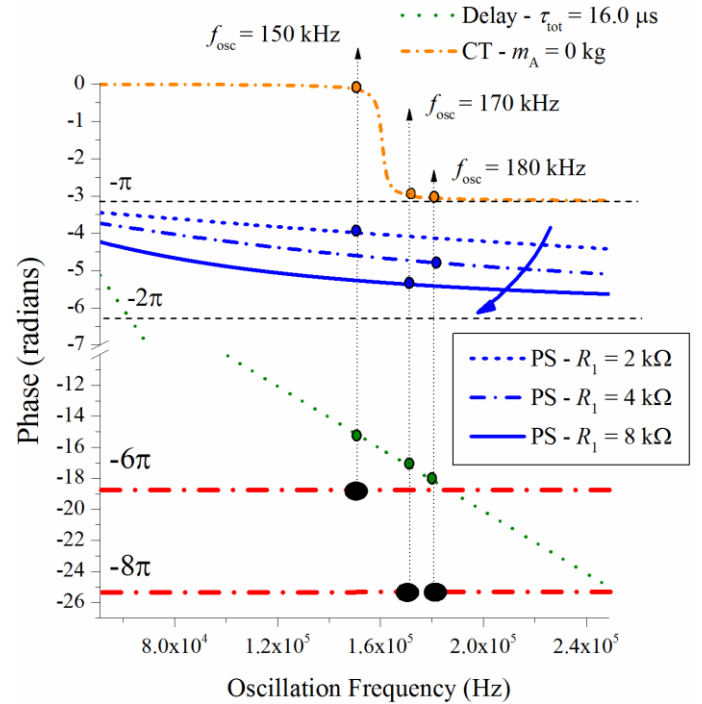


Fig. 6. Interpretation of one of the abrupt jumps in oscillation frequency measured experimentally using (13). This figure shows the phase associated to each element in the self-excitation loop (cantilever, phase-shifter and total intrinsic delay). The gain and saturator are not represented, since these elements act only on the amplitude of the signal and not on its phase. As shown in Fig. 4(a) and Fig. 5, the phase imposed in the loop by the phase-shifter can be controlled with the values of  $R_1$ , and the loop oscillation frequency adjusts to satisfy (13). The sudden jump corresponds to the change of the solution of (13) from  $-6\pi$  to  $-8\pi$  radians.

Fig. 6 illustrates the jump in oscillation frequency resulting from systematically increasing the values of the resistor  $R_1$ , as shown in Fig. 4(a) (for simplicity, only the first stage of the phase-shifter is considered with inverted polarity,  $P = -1$ ). It

can be observed that for a small value of  $R_1$  ( $R_1 = 2k\Omega$ , dotted blue line) the oscillation frequency solving (13) is given by  $f_{osc} = 150 \text{ kHz}$ , corresponding to a total phase shift of  $-6\pi$  radians. This frequency is lower than the natural resonance frequency of the cantilever with no added mass ( $f_0 = 162.32 \text{ kHz}$ ). An increment of  $R_1$  increases the shift introduced by the phase-shifter in the system. Therefore, the oscillation frequency is forced to decrease, and the magnitudes of the phase shifts introduced by the cantilever and total delay decrease as well to keep the sum constant at  $-6\pi$  radians. When this compensation is no longer possible (case of  $R_1 = 4k\Omega$ , dashed-dotted blue line) the system jumps to the solution  $-8\pi$  radians with an  $f_{osc} = 180 \text{ kHz}$ . After this point, the shifts to lower frequencies resume (case of  $R_1 = 8k\Omega$ , solid line,  $f_{osc} = 170 \text{ kHz}$ ), to compensate for the larger shift introduced by the phase-shifter. This process describes the shifts and jumps experimentally observed and plotted in Fig. 4 and Fig. 5.

#### D. Self-sustained oscillation frequency as function of added mass

Equation (13) allows to calculate the phase of the cantilever for each set of experimental conditions ( $R_1$ ,  $R_2$ ,  $p$ ) and for a self-sustained oscillation with frequency  $\omega_{osc}$ . Nevertheless, a systematic way of finding which multiple of  $-2\pi$  radians solves such phase condition is required. This task can be algorithmically performed by imposing the physical constraint that the cantilever phase must be in the range  $-\pi < \varphi_{CT} < 0$ , in agreement with the simple harmonic oscillator model. If the generic value  $\varphi_{elec}$  is written in the form  $\varphi_{elec} = a - n\pi$ , with  $0 < a < \pi$  and  $n = 1, 2, 3, \dots$ , the value of the cantilever phase is simply given by  $\varphi_{CT} = -a$ . Table III illustrates this procedure for some intervals of values of  $\varphi_{elec}$ , with specific examples.

By imposing that the phase  $\varphi_{CT} = -a$  of the cantilever oscillating in closed-loop at frequency  $\omega_{osc}$  is the same as the phase of the cantilever modelled as a damped harmonic oscillator in (7), one obtains:

$$\left( \frac{\omega_{osc}(c+c_{hydro})}{k-\omega_{osc}^2(0.24(m_{CT}+m_{hydro})+m_A)} \right) = -x \quad (14)$$

with  $x = \tan(\varphi_{CT})$ , and  $\varphi_{CT} = -a$ , calculated using the algorithm shown in Table III. Equation (14) can be rearranged in order to obtain an explicit dependence between the added mass,  $m_A$ , and the self-sustained oscillation frequency,  $\omega_{osc}$ :

$$m_A = \frac{(c+c_{hydro})}{\omega_{osc} x} + \frac{k}{(\omega_{osc})^2} - 0.24(m_{CT} + m_{hydro}). \quad (15)$$

TABLE III  
PHASE OF CANTILEVER,  $\varphi_{CT}$ , WORKING IN CLOSED-LOOP AS  
FUNCTION OF  $\varphi_{elec}$

$\varphi_{elec}$ (radians)		$\varphi_{elec} = a - n\pi$ $0 < a < \pi$ and $n = 1, 2, 3, \dots$		$\varphi_{CT} = -a$ (radians)
[0, $-\pi$ ]	$\varphi_{elec} = -1.0$	$\varphi_{elec} = a - \pi$	$\varphi_{elec} = 2.14 - \pi$	$\varphi_{CT} = -2.14$
	$\varphi_{elec} = -2.5$		$\varphi_{elec} = 0.64 - \pi$	$\varphi_{CT} = -0.64$
[ $-\pi$ , $-2\pi$ ]	$\varphi_{elec} = -3.5$	$\varphi_{elec} = a - 2\pi$	$\varphi_{elec} = 2.78 - 2\pi$	$\varphi_{CT} = -2.78$
	$\varphi_{elec} = -6.0$		$\varphi_{elec} = 0.28 - 2\pi$	$\varphi_{CT} = -0.28$
[ $-2\pi$ , $-3\pi$ ]	$\varphi_{elec} = -7.0$	$\varphi_{elec} = a - 3\pi$	$\varphi_{elec} = 2.42 - 3\pi$	$\varphi_{CT} = -2.42$
	$\varphi_{elec} = -8.5$		$\varphi_{elec} = 0.92 - 3\pi$	$\varphi_{CT} = -0.92$

Finally, the expressions for the hydrodynamics mass and damping coefficient, (2) and (3), can be introduced in (15) and an analytical expression relating the oscillation frequency of the cantilever vibrating in the feedback loop immersed in a viscous fluid and with a generic added mass is obtained:

$$m_A = \frac{1}{f_{osc} x} \left( \frac{c}{2\pi} + \frac{Lb_2\eta}{4} \right) + \frac{WL}{4} \sqrt{\frac{\rho\eta\pi}{f_{osc}}} \left( \frac{b_1}{x} - 0.24a_2 \right) + \frac{k}{(2\pi f_{osc})^2} - 0.24 \left( \frac{\pi}{4} \rho W^2 L a_1 - m_{CT} \right). \quad (16)$$

The intrinsic damping coefficient,  $c$ , is assumed constant for all range of added masses, which is an approximation (see the decrease of the quality factors,  $Q_A$ , with the increase in added mass in Table II). Nevertheless, while vibrating in air, the quality factors are high enough for this approximation to be reasonable. On the other hand, when the cantilever is immersed in a viscous fluid,  $c$  is negligible when compared with  $c_{hydro}$ .

According to the model developed here, (16) is a necessary condition for the existence of self-sustained oscillations in the feedback loop, but it does not provide any information on the stability of these solutions. This fact becomes relevant due to the presence of the periodic parameter  $x = \tan(\varphi_{CT})$  in (16). In this case, different values of oscillation frequencies  $f_{osc}$  will satisfy (16) for the same value of added mass  $m_A$ . The Nyquist Stability Criterion [43] can be used as a secondary criterion to assess the stability of the solutions: it states that the only stable solution of the system is the one with the highest real part of the transfer function  $G(j\omega) = pCT(j\omega)PS(j\omega)e^{-j\omega\tau_{tot}}$  (refer to [29, 30] for examples where this criterion has been successfully exploited to understand the stability of viscosity sensors).

The dependence of the oscillation frequency  $f_{osc}$  on the mass  $m_A$  attached to the cantilever, given by (16), is plotted on the left panel of Fig. 7. A constant value of  $R_1 = 0.02 \text{ k}\Omega$  and different values for  $R_2$  are considered in these examples, for both values of polarity. The geometrical and dynamical parameters of the cantilever reported in Table I and the rheological parameters of the air [40] were used in the model. In general, it can be observed that the oscillation frequencies decrease with the increase of the added mass, for the three different curves ( $R_2 = 10.12 \text{ k}\Omega$ ,  $R_2 = 0.32 \text{ k}\Omega$  and  $R_2 = 0.02 \text{ k}\Omega$ , respectively green, orange and purple lines). In addition, the solutions of (16) are shown to be periodic, with branches of solutions for different ranges of oscillation

frequencies. The sudden jumps of the oscillation frequencies observed experimentally correspond to a change of the solution branch, for a particular set of conditions. As explained, the real part of the transfer function  $G(j\omega)$  is plotted on the right side of Fig. 7, considering the same operating conditions, to help deciding the stability of each solution branch. To validate the detailed model, the values of oscillation frequencies measured experimentally using the same conditions than those used to plot (16) are presented in Table IV. This experimental data is added to Fig. 7 as colored circles and show a very good agreement with the respective modeled results. Finally, the dependence between the resonance frequency and the added mass of the same cantilever working in the traditional open-loop mode, given by (5), is also plotted in Fig. 7, for comparison with the closed-loop model.

Fig. 7(a) shows the case of non-inverted polarity ( $p = 1$ ). In this case, the solution of (16) is univocal for small added masses and there is no possible jump. For an added mass of  $m_A \sim 2.0 \times 10^{-12}$  kg a second branch of solutions of (16) appears at lower frequencies. A possible jump between these two solutions branches is then illustrated for  $m_A \sim 4.0 \times 10^{-12}$  kg (purple squares on top of the purple line of  $R_2 = 10.12$  k $\Omega$ ). In this case, the real part of the transfer function  $G(j\omega)$  becomes larger for the solution at  $f_{osc} = 124$  kHz than the solution at  $f_{osc} = 158$  kHz, and the former becomes the stable branch.

Fig. 7(b) shows the case of inverted polarity ( $p = -1$ ). The first thing that can be noted is that the solutions of oscillation frequencies are complementary to those shown in Fig. 7(a). In this case, the modeled operating conditions allow the occurrence of a jump at very small added masses ( $m_A \sim 2.0 \times 10^{-14}$  kg). This is the jump observed experimentally in Fig. 5 for the case of the small polystyrene bead (red circles). In addition, the jump shown in Fig. 5 for the case of the big glass bead (green squares) is also presented, for  $m_A \sim 1.5 \times 10^{-11}$  kg. Both jumps are indicated by the orange squares.

Fig. 7 shows that the results predicted by the proposed analytical model are in close agreement with the experimental measurements and that the model describes each aspect of the dynamical response of the system observed in Figs. 4 and 5. A deeper analysis of the model and data presented in this figure suggests the possibility of using this platform in three distinct ways, by adjusting the behavior of the sensor via  $R_1$ ,  $R_2$  and  $p$ . The first possibility is to use this device as a continuous mass sensor, whose oscillation frequency depends on the added mass to the cantilever. It is shown that for certain operating conditions, the response of this sensor follows the response of the microresonator working in open-loop (represented in Fig. 7 by the dashed-dotted magenta line representing (5)). Thus, the ultimate sensitivity of the sensor working in closed-loop is the same as the microresonator working in open-loop, but with better signal-to-noise ratio and resolution, typical of the closed-loop setups. In the case of this work, added masses of the order of  $10^{-14}$  kg (small polystyrene bead) were easily detected with a shift in frequency of around 150 Hz. Note that such added mass is well within the “flat” region of (5) (open-

loop mode), where small resonance frequency variations would be difficult to detect due to the poor signal-to-noise ratio associated with the typical open-loop setups.

TABLE IV  
EXPERIMENTALLY MEASURED DATA PLOTTED IN FIG. 7 AS  
COLORED CIRCLES

$R_1 = 0.02$ k $\Omega$ $R_2$ (k $\Omega$ )	No mass	Small Poly $\sim 2.0 \times 10^{-14}$ kg	Medium Poly $\sim 5.0 \times 10^{-13}$ kg	Big Poly $\sim 2.0 \times 10^{-12}$ kg	Big Glass $\sim 1.5 \times 10^{-11}$ kg
$p = 1$					
0.02	-	-	154.82 kHz	-	-
0.32	159.33 kHz	160.56 kHz	-	146.23 kHz	-
10.12	-	-	-	-	85.19 kHz
$p = -1$					
0.02	-	150.59 kHz	-	-	-
0.32	166.98 kHz	-	165.09 kHz	139.57 kHz	-
10.12	-	-	158.3 kHz	-	99.23 kHz

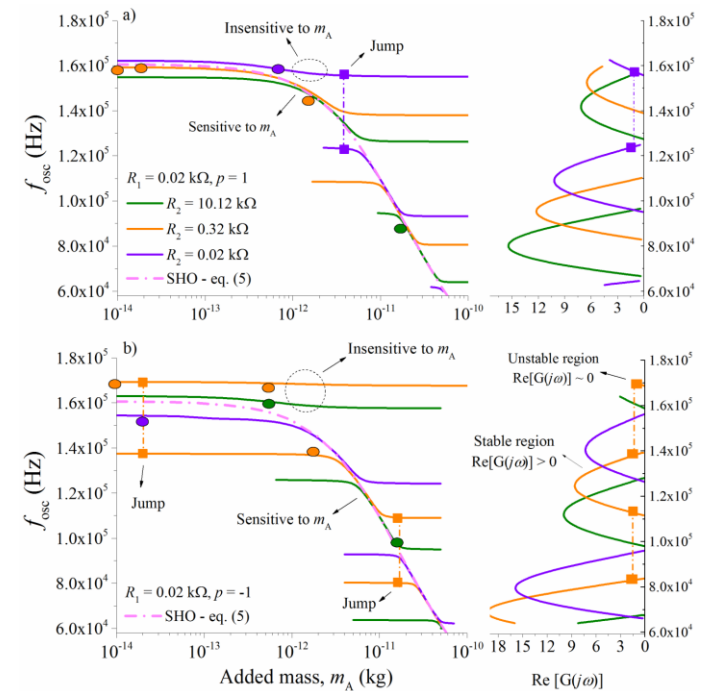


Fig. 7. Predictions of (16), showing the self-sustained oscillation frequencies as function of the mass added to the cantilever. Predictions from a simple externally excited harmonic oscillator given by (5) are shown with dashed lines, for comparison. a) Non-inverted polarity,  $p = 1$ ; b) Inverted polarity,  $p = -1$ . Insets on the right panel: real part of the transfer function  $G(j\omega) = pCT(j\omega)PS(j\omega)e^{-j\omega\tau_{tot}}$ , used to identify the stable solution according to the Nyquist Stability Criterion. The coloured circles indicate the respective experimental measurements (Table IV), while the squares indicate possible jumps. Three potential working modalities (continuous sensor, threshold sensor and stable resonator) are illustrated.

The second possibility is to use this platform as a threshold sensor, in which a small variation of mass causes a sudden jump of the oscillation frequencies. Furthermore, it is shown that the location of the abrupt jump can be positioned in the range of added masses of interest by controlling the operating conditions, and in particular by tuning the potentiometers  $R_1$  and  $R_2$  in the phase shifter.

Finally, the third possible way of operating this platform is as a stable microresonator, whose oscillation frequency is almost unaffected by the added mass. Fig. 7 shows regions where the oscillation frequency of the resonator completely deviates from the response characteristic of the open-loop mode, given by (5), and is almost constant for a wide range of added masses. A resonator insensitive to environmental conditions can be used for applications where, for example, a stable signal is required for precision timing and frequency references [44]. In reference [30] it was shown that, for specific operating conditions of this platform, the microresonator can also be insensitive to the viscosity of the medium. Such a device could therefore potentially be used to decouple the effect of simultaneous external factors acting on the resonator, for example a chemical reaction where the added mass to the cantilever and the viscosity of the medium change simultaneously [45].

## V. CONCLUSIONS

The dynamical response of a microcantilever self-oscillating in a feedback loop is experimentally studied as a function of the mass added to the cantilever and as a function of the phase shift of the signal along the loop. An analytical model capable of explaining the observed phenomena is proposed by describing the microcantilever as a variable mass harmonic oscillator immersed in a viscous fluid and by exploiting a phase condition for the existence of self-sustained oscillations. The experimental and modeled results suggest that this platform can be used in three distinct modes, according to the chosen operating conditions. The first working mode is continuous mass sensing. In this case, the oscillation frequency changes smoothly with the mass added to the cantilever, in a similar fashion and with the same ultimate sensitivity as the cantilever working in traditional open-loop mode. Nevertheless, the closed-loop scheme allows obtaining a better resolution and signal-to-noise ratio than the traditional open-loop technique. The second working mode is threshold mass sensing. In this case, an arbitrarily small added mass can induce a sudden jump of the oscillation frequency. Furthermore, the location of the abrupt jump can be positioned in the range of added masses of interest by controlling the phase of the cantilever with the adjustable phase-shifter. This feature can be extremely useful in applications such as point-of-care diagnosis, where the presence of an analyte of interest above a certain concentration must be assessed. Finally, this platform can also work as a stable microresonator, whose oscillation frequency is unaffected by some environmental condition (added mass, viscosity or density). This feature can prove to be extremely important in applications where a stable resonance frequency, independent of the external factors, is required, or to decouple the effect of competing external parameters on the dynamical response of the resonator. These degrees of flexibility are not available with current microcantilever-based mass sensors.

## ACKNOWLEDGMENT

The authors wish to thank Elbatech srl for the support in the design and realization of the self-excitation electronics. The data presented in this paper are freely available at <https://doi.org/10.5281/zenodo.1095581>.

## REFERENCES

- [1] K. L. Ekinci and M. L. Roukes, "Nanoelectromechanical systems", *Review of Scientific Instruments* vol. 76, pp. 061101-1-061101-12, 2005.
- [2] L. Manning, B. Rogers, M. Jones, J. D. Adams, J. L. Fuste and S. C. Minne, "Self-oscillating tapping mode atomic force microscopy", *Review of Scientific Instruments*, vol. 74 no. 9, pp. 4220-4222, 2003.
- [3] J. Moser, J. Güttinger, A. Eichler, M. J. Esplandiú, D. E. Liu, M. I. Dykman and A. Bachtold, "Ultrasensitive force detection with a nanotube mechanical resonator", *Nature Nanotechnology*, vol. 8, pp. 493-496, 2013.
- [4] N. Belminoud, I. Dufour, A. Colin and L. Nicu, "Rheological behaviour probed by vibrating microcantilevers", *Applied Physics Letters*, vol. 92, pp. 041907-1-041907-3, 2008.
- [5] X. C. Zhang, E. B. Myers, J. E. Sader and M. L. Roukes, "Nanomechanical torsional resonators for frequency-shift infrared thermal sensing", *Nanoletters*, vol. 13, no. 4, pp. 1528-1534, 2013.
- [6] K. L. Ekinci, W. T. Yang and M. L. Roukes, "Ultimate limits to inertial mass sensing based upon nanoelectromechanical systems", *Applied Physics Letters*, vol. 95, no. 5, pp. 2682-2689, 2004.
- [7] J. Chaste, A. Eichler, J. Moser, G. Ceballos, R. Rurali and A. Bachtold, "A nanomechanical mass sensor with yoctogram resolution", *Nature Nanotechnology*, vol. 7, pp. 301-304, 2012.
- [8] T. R. Albrecht, P. Grutter, D. Horne and D. Rugar, "Frequency modulation detection using high-Q cantilevers for enhanced force microscope sensitivity", *J. Appl. Phys.* vol. 69, no.2, pp. 668-673, 1991.
- [9] J. Tamayo, M. Alvarez and L. M. Lechuga, "Digital tuning of the quality factor of micromechanical resonant biological detectors", *Sensors and Actuators B*, vol. 89, pp. 33-39, 2003.
- [10] B. Gotsmann and H. Fuchs, "Dynamic AFM using the FM technique with constant excitation amplitude", *Applied Surface Science* vol. 188, no. 3, pp. 355-362, 2002.
- [11] S. Dohn, S. Schmid, F. Amiot and A. Boisen, "Position and mass determination of multiple particles using cantilever based mass sensors", *Applied Physics Letter*, vol. 97, pp. 044103-1-044103-3, 2010.
- [12] D. Ossola, P. Dorig, J. Voros, T. Zambelli and M. Vassalli, "Serial weighting of micro-objects with resonant microchanneled cantilevers", *Nanotechnology*, vol. 27, pp. 415502-1-415502-10, 2016.
- [13] J. Lee, W. Shen, K. Payer, T. P. Burg and S. R. Manalis, "Toward attogram mass measurements in solution with suspended nanochannel resonators", *Nano Letters*, vol. 10, no. 7, pp. 2537-2542, 2010.
- [14] Y. Weng, F. F. Delgado, S. Son, T. Burg, S. C. Wasserman and S. R. Manalis, "Mass sensors with mechanical traps for weighing single cells in different fluids", *Lab on a Chip*, vol. 11, pp. 4174-4180, 2011.
- [15] T. R. Rodríguez and R. García, "Theory of Q control in atomic force microscopy", *Applied Physics Letters*, vol. 82, no. 26, pp. 4821-4823, 2003.
- [16] G. Prakash, S. Hu, A. Raman and R. Reifengerger, "Theoretical basis of parametric-resonance-based atomic force microscopy", *Physical Review B*, vol. 79, pp. 094304-1-094304-10, 2009.
- [17] G. Prakash, A. Raman, J. Rhoads and R. Reifengerger, "Parametric noise squeezing and parametric resonance of microcantilevers in air and liquid environments", *Review of Scientific Instruments*, vol. 83, pp. 065109-1-065109-12, 2012.
- [18] M. Basso, P. Paoletti, B. Tiribilli and M. Vassalli, "Modelling and analysis of autonomous micro-cantilever oscillations", *Nanotechnology*, vol. 19, pp. 475501-1-475501-8, 2008.
- [19] M. Basso, P. Paoletti, B. Tiribilli B and M. Vassalli, "AFM imaging via nonlinear control of self-driven cantilever oscillations", *IEEE Transactions on Nanotechnology*, vol. 10, no. 3, pp. 560-565, 2011.
- [20] K. L. Ekinci, M. H. Huang and M. L. Roukes, "Ultrasensitive nanoelectromechanical mass detection", *Applied Physics Letters*, vol. 84, no. 22, pp. 4469-4471, 2004.



- [21] Y. T. Yang, C. Callegari, X. L. Feng, K. L. Ekinici and M. L. Roukes, "Zeptogram-scale nanomechanical mass sensing", *Nano Letters* vol. 6, no. 4, pp. 583-586 2006.
- [22] A. K. Naik, M. S. Hanay, W. K. Hiebert, X. L. Feng and M. L. Roukes, "Towards single-molecule nanomechanical mass spectrometry", *Nature Nanotechnology*, vol. 4, pp. 445-450, 2009.
- [23] S. Olcum, N. Cermak, S. C. Wasserman and S. R. Manalis, "High-speed multiple-mode mass-sensing resolves dynamic nanoscale mass distributions", *Nature Communications*, vol. 6, no. 7070, pp. 1-8, 2015.
- [24] H. K. Lee, R. Melamud, S. Chandorkar, J. Salvia, S. Yoneoka and T. W. Kenny, "Stable operations of MEMS Oscillators far above the critical vibration amplitude in the nonlinear regime", *Journal of Micromechanical Systems*, vol. 20, no. 6, pp. 1228-1230, 2011.
- [25] V. Zega, S. Nitzan, M. Li, C. H. Ahn, E. Ng, V. Hong, Y. Yang, T. Kenny, A. Corigliano and D. A. Horsley, "Predicting the closed-loop stability and oscillation amplitude of nonlinear parametrically amplified oscillators", *Applied Physics Letter*, vol. 106, pp. 233111-1-233111-5, 2015.
- [26] W. J. Venstra, H. J. R. Westra and H. S. J. van der Zant, "Mechanical stiffening, bistability, and bit operations in a microcantilever", *Applied Physics Letters*, vol. 97, pp. 193107-1-193107-3, 2010.
- [27] R. van Leeuwen, D. M. Karabacak, H. S. J. van der Zant and W. J. Venstra, "Nonlinear dynamics of a microelectromechanical oscillator with delayed feedback", *Physical Review B*, vol. 88, pp. 214301-1-214301-5, 2013.
- [28] R. M. C. Mestrom, R. H. B. Fey and H. Nijmeijer, "Phase feedback for nonlinear MEM Resonators in oscillator circuits", *IEEE/ASME Transactions on Mechatronics*, vol. 14, no. 4, pp. 423-433, 2009.
- [29] J. Mouro, B. Tiribilli and P. Paoletti, "Nonlinear behaviour of self-excited microcantilevers in viscous fluids", *Journal of Micromechanics and Microengineering*, vol. 27, pp. 095008-1-095008-12, 2017.
- [30] J. Mouro, B. Tiribilli and P. Paoletti, "Measuring viscosity with nonlinear self-excited microcantilevers", *Applied Physics Letters*, vol. 111, pp. 144101-1-144101-4, 2017.
- [31] M. S. Hanay, S. I. Kelber, C. D. O'Connell, P. Mulvaney, J. E. Sader and M. L. Roukes, "Inertial imaging with nanomechanical systems", *Nature Nanotechnology*, vol. 10, no. 4, pp. 339-344, 2015.
- [32] D. Nečas and P. Klapetek, "Gwyddion: an open-source software for SPM data analysis", *Cent. Eur. J. Physics*, vol. 10, no. 1, pp. 181-188, 2012.
- [33] Density of polystyrene beads:  
<http://www.sigmaaldrich.com/catalog/product/sial/72986?lang=pt&region=PT> (Last accessed: 07 December 2017)
- [34] Density of glass beads:  
<http://www.whitehousescientific.com/ekmps/shops/whisci/resources/Other/technical-specification-for-sodalime-glass.pdf> (Last accessed: 07 December 2017)
- [35] M. Bao, "Stress and strain of beam structures", in *Analysis and Design Principles of MEMS Devices*, 1st ed., Amsterdam, The Netherlands, Elsevier, 2005, pp. 46-63.
- [36] J. L. Sader, "Frequency response of cantilever beams immersed in viscous fluids with applications to the atomic force microscope", *Journal of Applied Physics*, vol. 84, no. 1, pp. 64-76, 2008.
- [37] A. Maali, C. Hurth, R. Boisgard, C. Jai, T. Cohen-Bouhacina and J-P. Aimé, "Hydrodynamics of oscillating atomic force microscopy cantilevers in viscous fluids", *Journal of Applied Physics*, vol. 97, pp. 074907-1-074907-6, 2005.
- [38] I. Dufour, A. Maali, Y. Amarouchene, C. Ayela, B. Caillard, A. Darwiche, M. Guirardel, H. Kellay, E. Lemaire, F. Mathieu, C. Pellet, D. Saya, M. Yousry, L. Nicu and A. Colin, "The microcantilever: a versatile tool for measuring the rheological properties of complex fluids", *Journal of Sensors*, vol. 2012, 719898, 2012.
- [39] V. Kaajakari, T. Mattila, A. Oja and H. Seppa, "Nonlinear limits for single-crystal silicon microresonators", *Journal of Micromechanical Systems*, vol. 13, no. 5, pp. 715-724, 2004.
- [40] Properties of the air: [http://www.engineeringtoolbox.com/air-properties-d\\_156.html](http://www.engineeringtoolbox.com/air-properties-d_156.html) (Last accessed: 07 December 2017)
- [41] S. Dohn, W. Svendsen, A. Boisen and O. Hansen, "Mass and position determination of attached particles on cantilever based mass sensors", *Review of Scientific Instruments*, vol. 78, pp. 103303-1-103303-3, 2007.
- [42] G. Y. Chen, R. J. Warmack, T. Thundat, D. P. Allison and A. Huang, "Resonance response of scanning force microscopy cantilevers", *Review of Scientific Instruments*, vol. 65, no. 8, pp. 2532-2537, 1994.
- [43] H. K. Khalil, "Frequency domain analysis of feedback systems", in *Nonlinear Systems*, 3rd ed., Upper Saddle River, NJ: Prentice-Hall, 2002, pp. 263-296.
- [44] C. M. Jha, J. Salvia, S. A. Chandorkar, R. Melamud, E. Kuhl and T. W. Kenny, "Acceleration insensitive encapsulated silicon microresonator", *Applied Physics Letters*, vol. 93, pp. 234103-1-234103-3, 2008.
- [45] I. Dufour, F. Josse, S. M. Heinrich, C. Lucat, C. Ayela, F. Ménéil and O. Brand, "Unconventional uses of microcantilevers as chemical sensors in gas and liquid media", *Sensors and Actuators B*, vol. 170, pp. 115-121, 2012.



**João Mouro** received the Master's degree in Chemical Engineering, in 2010, and the PhD in Technological Physics Engineering, in 2015, both from Instituto Superior Técnico, Lisbon, Portugal. From July 2016 through July 2017 he was a Postdoctoral Researcher at the University of Liverpool (UK), and he is currently a Postdoctoral Researcher at the Department of Electrical and Electronic Engineering at the University of Bristol, United Kingdom. His main interests include the design, fabrication and modeling of non-linear MEMS systems, for sensing and switching applications.



**Bruno Tiribilli** graduated in Physics at the University of Florence in 1985, with a thesis on holographic moiré topography. In 1989 he became optics specialist. At the beginning of his career he was employed in a space industry, in charge of the design and construction of optoelectronic systems for satellite attitude sensors. In 1990 he became a researcher at National Institute of Optics, his activities concerned the design and realization of optical instruments for scientific and industrial application, including several international collaboration. Since 2005 he is a senior researcher at the ISC-CNR (Institute for Complex Systems of the National Research Council). His current activity mainly focuses on the design and development of atomic force microscopy instrumentation for applications in biology and biophysics.



**Paolo Paoletti** is a Senior Lecturer in Control at the University of Liverpool (UK). He graduated in Automation Engineering (2006) and obtained a PhD in Nonlinear Dynamics and Complex Systems (2010) from the University of Florence, Italy. Before joining the University of Liverpool, he worked as research assistant at the Italian Institute for Complex Systems (2010), and as postdoctoral fellow at the School of Engineering and Applied Science, Harvard University (2010-2012). Dr. Paoletti's research interests lie in nonlinear dynamics and control, with a special focus on problems that sit at the boundary between different traditional disciplines such as biology, robotics, computer science, mathematics and physics. In 2014 he was awarded the "Rising Star" award from the UK Engineering and Physical Sciences Research Council.